STTR Final Scientific/Technical Report Submitted to Department of Energy

DOE Award Number:	**DE-SC0004702**
Project Title:	**Femtosecond Timing Distribution and Control for Next Generation Accelerators and Light Sources**
Principal Investigator:	**Dr. Li-Jin Chen** **CEO** **Idesta Quantum Electronics, LLC** **l.chen@idestaqe.com** **(973)-300-4362**
Submission Date:	**Mar 31st, 2014**
Recipient Organization:	 **Idesta Quantum Electronics, LLC** **56 Sparta Avenue** **Newton, NJ, 07860**
Project Period:	**Year 1: 08/15/2011 – 08/14/2012** **Year 2: 08/15/2012 – 12/31/2013**
Report Term:	**Final Report of STTR Phase II Award**

Femtosecond Timing Distribution and Control for Next Generation Accelerators and Light Sources

I. Executive Summary

The emergence of few fs x-ray pulses generated from state-of-the-art XFELs has enabled the study of ultrafast phenomenon using optical/x-ray pump-probe techniques. In many time-resolved experiments, timing synchronization of x-ray and optical pulses with a precision of or below 10 fs is required. Traditional and widely deployed rf-based synchronization systems are only capable of providing timing signal with an rms error of around 100 fs. The next generation of future light sources such as the LCLS-II producing sub-femtosecone X-ray pulses will further increase the need for precision timing of the entire accelerator facility. In this STTR grant, Idesta Quantum Electronics (idestaQE), LLC has closely collaborated with the Linac Coherent Light Source (LCLS) at Stanford Linear Accelerator Center (SLAC) to carry out an extensive study on an advanced large-scale, drift-free timing distribution and synchronization system based on femtosecond mode-locked Erbium fiber laser. For the first time, a 3.3fs rms timing drift over 24 hours of operation has been achieved in synchronization of a remote Ti:sapphire laser to the timing of the optical master oscillator (OMO) delivered by a 360 meter long timing stabilized, dispersion compensated fiber link where the OMO is synchronized to the rf master oscillator (RMO). Critical parameters has been identified and can provide important guide-lines necessary for further optimization for the future upgrading to even sub-fs precision level.

Three key timing modules have been developed within this project – (1) A **B**alanced **O**ptical-**M**icrowave **P**hase **D**etector (BOM-PD), a fiber Sagnac-based interferometer for detecting phase error between optical and microwave oscillators and performing synchronization; (2) A **F**iber **L**ink **S**ystem (FLS) based on PPKTP **B**alanced **O**ptical **C**rosscorrelator (PPKTP-BOC) for stabilizing the length of timing distribution fibers; (3) A **T**wo-**C**olor **B**alanced **O**ptical **C**rosscorrelator (TC-BOC) for detecting phase error between an femtosecond Er-fiber laser oscillator and a Ti:sapphire laser and performing synchronization. These modules have been tested both individually and together in this project and proven to be capable of delivering sub-10fs timing precision. Comparing to other high-precision optical timing systems, our system is not only cost competitive but provides a complete solution for timing distribution and synchronization of both microwave and optical oscillators at sub-10 fs level.

Delivering the first sub-10 fs timing infrastructure to an active XFEL-facility is an important milestone in the development of the next-generation x-ray sources and might provide LCLS or LCLS-II a competitive edge against other FEL based light sourced around the globe. Moreover, large-scale timing synchronization technology can also be applied in other facilities such as the National Ignition Facility (NIF) for synchronizing multiple powerful laser beams to reach extreme levels of energy and peak power on a target for studying fusion ignition. In addition, the unique optical-to-optical synchronization modules based on BOCs can be a sold as a commercial product to the general ultrafast community, especially the upcoming optical parametric chirped pulse amplifier systems currently under active development.

II. Comparison of the actual accomplishments with the goals and objectives of the project

The proposed system in this project was targeted for a long-term stability better than 10 fs rms over 24 hours and a timing jitter below 10 fs in the 10 Hz – 10 MHz range. To accomplish this goal, we proposed an optical timing distribution system for LCLS as outlined in Figure 1. In the original design, the OMO with a repetition rate of 119 MHz (24th sub-harmonic of the 2856 MHz rf clock signal) was phase locked to the LINAC main drive line at 2865 MHz using the under Phase I optimized BOM-PD. The OMO repetition rate was later revised to 68MHz (42th sub-harmonic of the 2856 MHz rf clock signal) in order to be phase locked to the RMO at 476 MHz which was more easily available during the period of the project. The trade-off was that such decrease of oscillator frequencies even increased the difficulty in precise synchronization. In the accelerator environment, one main challenge was that the rf-pickup cavity is located at the end of the LINAC just before the electrons enter the undulator where access was highly restricted and the area was subject to intense radiation. The OMO therefore needed to be located in the laser room about 300 meters away from the rf pickup. As a result, a timing-stabilized optical link was needed to run between the laser room and the rf-pickup location. The error signal generated by the BOM-PD can be transmitted easily by copper cable back to the OMO. After amplification in an EDFA the pulses from the OMO will be distributed via stabilized optical fiber links to the modelocked laser oscillators and amplifiers in the remote location. A two color (1550 nm and 800 nm) balanced optical cross-correlator was used to compare the timing of the optical pulses produced by the Ti:Sa lasers to the pulses coming from the OMO and therefore ultimately to the LCLS rf-clock. Such two-color BOC also allowed recording the synchronization between the X-ray pulse and the ultrafast optical pulses immediately before they interact with the target. Having time stamps for each element in the ultrafast pulse chain given by the Ti:Sa oscillator, the amplifier, and the pulse arrival in the hutch allowed also to identify sources of jitter within this chain.

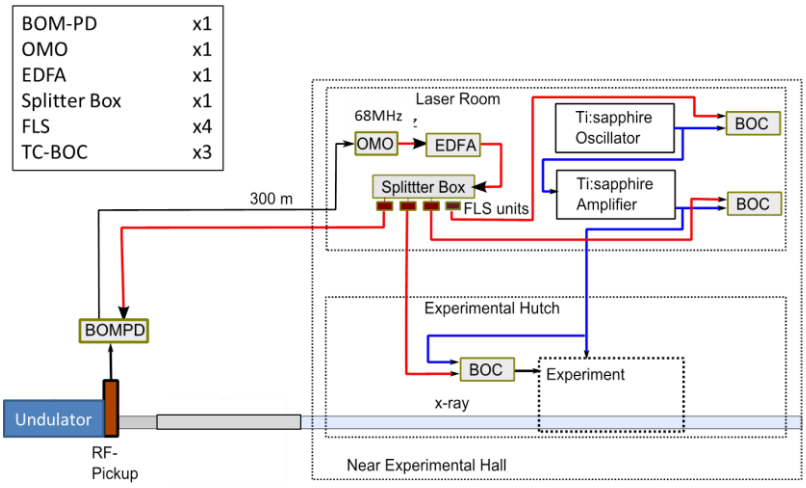

Figure 1: Layout of timing system to be installed at SLAC

To realize such an ideal timing systems described above, we identified a list of tasks to be pursued during this two-year phase II STTR project. The original objectives and goals of the tasks and actual accomplishments are summarized below:

Task 1: Development of a two color, two stage balanced cross-correlator to optically synchronize (TCBOC) a laser end station to the Optical Master Oscillator (OMO)

In order to optically synchronize the lasers in the laser room and experimental hutches to the OMO, we developed a customized TC-BOC adapted to produce an error signal from two different wavelengths, namely 1550 nm and 800 nm. The challenges here are not only in the two-color design but also in making the device long term stable as the two pulses need to stay overlapped in space and time. IdestaQE has put into intensive engineering efforts from the beginning of this project in designing and commercializing the TC-BOC (Fig. 2) needed for this project. Several TC-BOCs has been built and delivered to LCLS for performing optical-to-optical synchronization and timing error characterization between OMO and Ti:sapphire oscillators. Locking of the Ti:sapphire laser to the OMO is very important for time-resolved optical/x-ray pump probe experiment. In our system, we locked the Ti:sapphire laser to the OMO by a TC-BOC, which acted as an optical mixer and used the balanced detection to suppress against AM-to-PM conversion. The typical performance of our TC-BOC is shown in Fig. 3 which shows a timing sensitivity of 14mV/fs using 7 mW input power from the OMO and 100 mW power from the Ti:sapphire oscillator. The 1550 nm and the 800 nm light were mixed in a barium borate (BBO) crystal to produce the forward and backward cross-correlation traces. The difference between two time-delayed cross-correlations produces the s-curve which maps the timing jitter into a voltage signal. The linear region of the s-curve is designed to be around 500 fs.

Figure 2: Photo of IdestaQE's TC-BOC (commercially available)

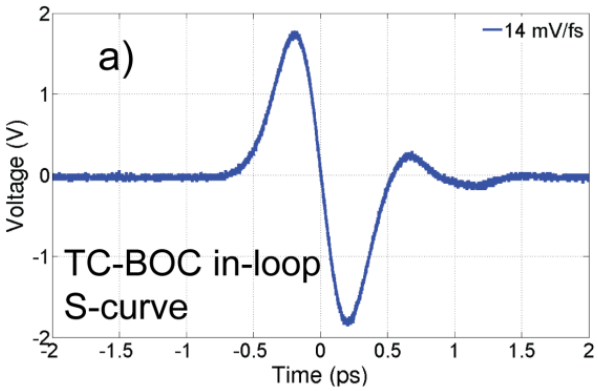

Figure 3: Typical performance of TC-BOC designed by IdestaQE.

Task 2: Timing error monitor interface development in order to integrate the optical timing system into the accelerator control system

In order to create reliable time stamping and to allow for easy post processing of the recoded pump probe data. IdestaQE and PULSE/LCLS has collaborated to interface the timing system with LCLS control and data acquisition system. We have developed an error monitor software that provides an easy-to-use interface for controlling the slow feedback loops in the timing system, as well as providing a quick overview on the functioning of various components in the timing system. The software uses a Labjack U6 Pro DAQ to monitor the control loops outputs from one FLS and one TCBOC, and if necessary it would move the slow delay lines to center the error signals for the corresponding optical-correlator. Monitoring the OMO-BOMPD control loop was also realized using the data acquisition function of the software. For long term evaluation of the timing system, data logging of the control loops outputs, time stamps, and stage positions are recorded once per second or other desired sampling rate into a csv file. A screenshot of the timing error monitor program is shown in Fig. 4. The program was written in MATLAB for easy integration with LCLS' existing software interface. The source code has been shared with the LCLS group.

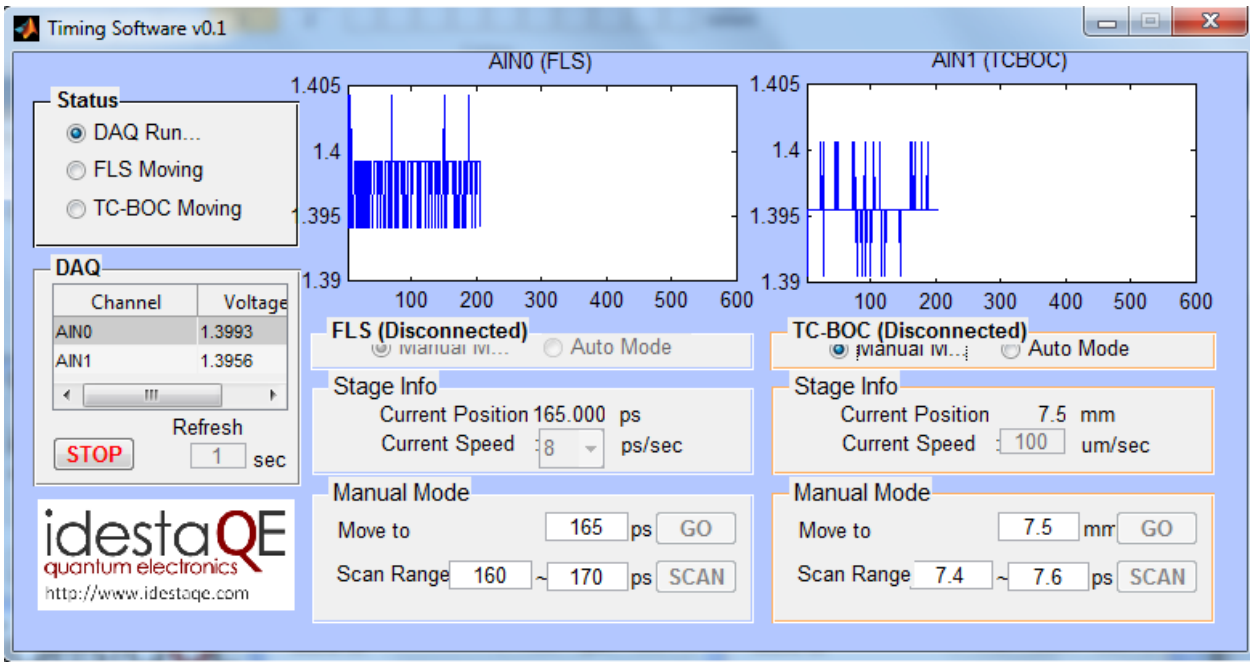

Figure 4 - Screen shot of the timing error monitor software developed at IdestaQE

Task 3: Low Offset-drift, low noise, high-bandwidth feedback electronics

Feedback controllers are one of the key components in timing systems. A proportional-integral (PI) or a proportional-integral-derivative (PID) is often used to close the phase-locked loops which synchronize the free-running oscillators or other devices to be stabilized. The ideal feedback controller should be zero offset-drift, noise-free, and high-bandwidth in order to achieve the best performance in timing synchronization of various oscillator and timing distribution. Therefore, suitable feedback electronics must be identified and used to realize the sub-10fs timing precision goal proposed in the project. Since there were already many candidate controllers on the market that might meet our needs, our plan was changed to identify one commercially-available feedback controller suitable for our purpose instead of developing on our own a new feedback controller as originally proposed. We obtained two types of analog controllers from Stanford Research Systems (SIM960 PID controller) and Newport (LB-1005 PI controller) and performed tests. Both controllers have large enough output bandwidth (100kHz for SIM960 and 10MHz for LB-1005) and comparable noise performance during short-term operation. The SIM960 has two useful features that LB-1005 lacks – (1) communication with computer via RS-232; (2) more flexible tuning with the additional derivative parameter. However, we found that SIM960 occasionally produced random pulsed noise which contaminate the signal. Therefore, we have decided to use all LB-1005 as the feedback controllers in our system and build the whole control electronics loop around them.

Task 4: Building the system: Erbium-doped Fiber Amplifier (EDFA), Balanced Optical Microwave Phase Detector (BOM-PD), Fiber length Stabilization (FLS) and TC-BOC

Task 4 was the main focus during the first year. IdestaQE proposed to build and pre-test the key components including a BOM-PD customized to the SLAC clock frequency (476 MHz), several

PPKTP-BOCs, and TC-BOCs for building the proposed system. Figure 5 and 6 show the pictures of the latest version of IdestaQE's BOM-PD with its dedicated temperature controller and the PPKTP-BOC used in the fiber-link system.

Figure 5: Photo of IdestaQE's BOM-PD (top) and its dedicated temperature controller (bottom).

Figure 6: Photo of IdestaQE's PPKTP-BOC.

In the original plan, the OMO, the EDFAs and the splitter box will be sourced from a third-party vendor. However, we have later decided to build the EDFAs and splitter box on our own since special care needs to be taken to handle the nonlinearity caused by the high-peak-power pulses delivered by the OMO. For the OMO, a customized fiber laser from Toptica (FemtoErb 1560nm)

was selected due to its extremely stable mode-locking performance. The OMO has an average output power of >80 mW and FWHM pulse width of around 200 fs at a repetition rate of around 68 MHz. Erbium doped femtosecond fiber laser is the ideal candidate for the OMO due to the availability of many extremely reliable telecom-components. In order to qualify as a real OMO for SLAC, the laser needs to work reliably and hands-off for months and years. We have also established a numerical tool which can be used to simulate the nonlinear pulse propagation inside the optical fibers. The simulation results are used to evaluate different system configurations. The numerical integration technique used is a 4^{th}-order Runge-Kutta method in the interaction picture with adaptive step-size control. Important nonlinear effects such as self-phase modulation (SPM), stimulated Raman scattering (SRS), and self-steepening (SS) are all taken into account in the numerical model. The model is very useful for providing guidelines for fiber dispersion and nonlinearity management. The power splitter box, which is used to divide the OMO power into multiple channels used for different applications, is based on a free-space design where the splitting ratio can be arbitrarily adjusted by rotating the polarization of the input beam before the polarization beamsplitter. In order to minimize the relative timing drifts between different channels, the splitter was built on symmetric building blocks so each output has almost identical path length from the input. These modular breadboards are made of magnetic stainless steel to further minimize the temperature effects on power and timing stability. The free-space design also prevents each channel from having power-dependent nonlinear effects. Figure 7 shows the picture of an 1x4 power splitter designed for this project.

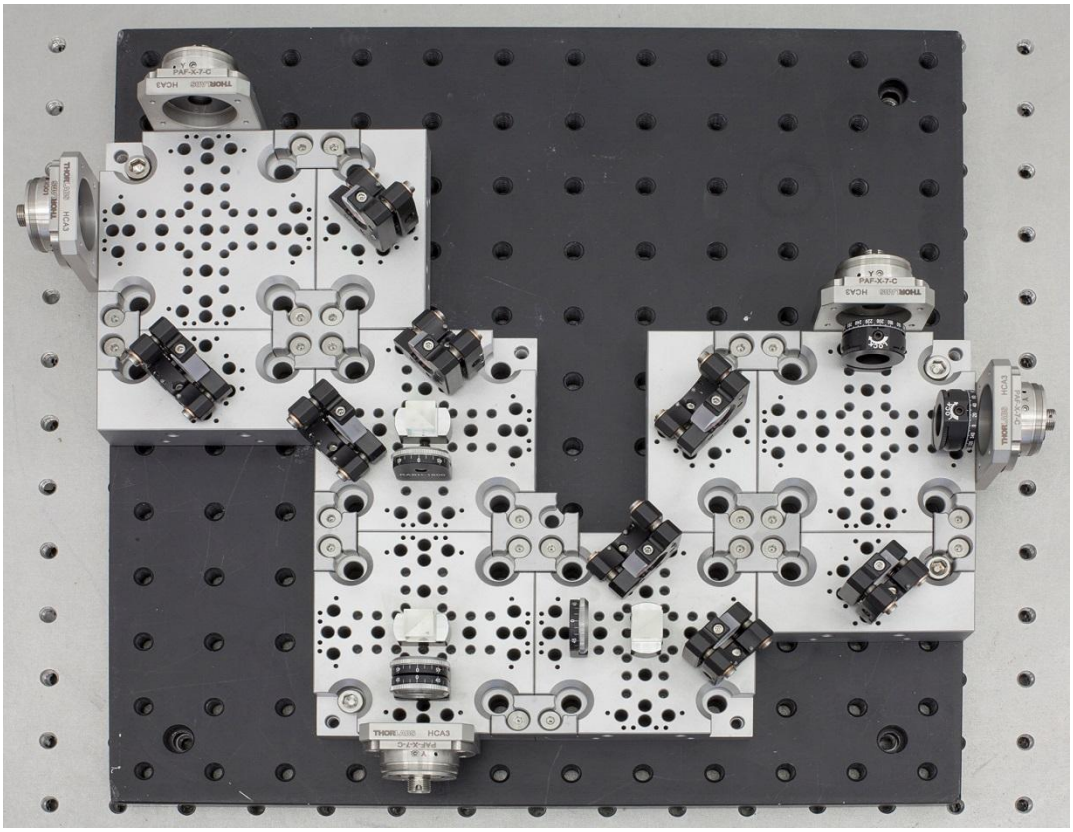

Figure 7: Photo of IdestaQE's 1x4 free-space power splitter with variable splitting ratio.

Task 5: Conditioning LCLS for new timing system

Simultaneously with Task 4, LCLS started to identify necessary modifications of its existing hardware and condition the laboratory environment to accommodate the fs-laser based timing distribution system. First of all, an ultra-low timing jitter local oscillator from Wenzel at 476 MHz (6th subharmonic of 2856 MHz) was used as the radio-frequency master oscillator (RMO), instead of the actual accelerator RF pick-up from the phase cavity which was not always accessible. Several broadband Ti:sapphire lasers from Femtolaser as well as Coherent operated at the same repetition rate (~68MHz) were used to test the system performance when synchronized to the OMO. A home-built pre-synchronization box based on the traditional photodetection technique was also built to assist the characterization of TC-BOC performance. The experiments were carried out in the Research Laser Lab (RLL) of the Near Experimental Hall (NEH). In addition, a dedicated computer loaded with all control and data acquisition software was prepared to record the long-term stability of the system. Several temperature and humidity sensors were also installed to monitor the environmental changes of the laboratory during the experiment.

Task 6: Installation at LCLS

In the original proposal, IdestaQE and LCLS planned to install the fs-laser-based timing distribution system in the NEH with an ultimate goal of running the timing link fibers through the accelerator tunnel. However, the work schedule needs to be compliant with the accelerator schedule as parts of the work can only be performed while the machine is down. Unfortunately, due to several irresistible reasons including government shutdown and schedule conflicts with other LCLS projects, the timing link fibers were not yet installed by the end of the project period. As a result, all the experiments were carried out in the RLL. The performance tests were done with the link fibers removed from the spool and loosely placed on the table. The results will be discussed in the next section.

Task 7: Hardware test and identification of potential electromagnetic interferences at LCLS

In the original proposal, we planned to test all delivered hardware in the accelerator environment to identify possible interferences with other electronic and optical signals present in the accelerator environment and experimental halls at LCLS. However, due to the reason addressed above, we were only able to perform the hardware test and identify the electromagnetic interference.in the NEH only.

Task 8: Verification of the timing distribution system at LCLS

This task will be the main focus for the second year. As planned in the project, a series of long and short term measurements were conducted to verify the performance of the timing distribution system. Comparing to other already existing approaches, we have demonstrated the first remote optical synchronization of a Ti:sapphire laser to the OMO/RMO via a timing-stabilized fiber link based on a PPKTP-BOC and a TC-BOC. The OMO is stabilized to the RMO using a BOM-PD. The out-

of-loop measurement showed a long-term timing stability of 3.3fs rms drifts over 24 hours of operation, as promised in the proposal.

III. Summary of Project Activities

During the first year of the project, IdestaQE delivered one OMO, one BOM-PD with temperature controller, two FLS, and two TCBOC (one in-loop, one out-of-loop version) to LCLS for preliminary testing. Preliminary component tests, as well as system test on one timing link, were carried out in the NEH Research Laser Lab (RLL) in preparation of the installation at the intended location inside the laser hall. The progress made during this period is summarized below.

III.1. Optical Master Oscillators (OMO)

Erbium doped femtosecond fiber lasers are the ideal candidates for the OMO due to the availability of many extremely reliable telecom-components. In order to qualify as a real OMO for SLAC, the laser needs to work reliably and hands-off for months and years. IdestaQE did evaluate commercially available fiber lasers with respect to their reliability and jitter performance. Among these, the fiber laser from Toptica (FemtoErb 1560nm) was selected as the OMO for this project due to the extremely stable mode-locking performance of these lasers.

In the previous progress report, we found that significant optical spectrum distortion was present in the fiber link due to self-phase modulation. The strong nonlinearity was due to the high peak power from the relatively low repetition rate and short pulses from the broadband OMO. Therefore, additional efforts were spent together with Toptica to customize the OMO to obtain a narrower spectrum. The resulting modifications lead to a spectral width of 28.5 nm FWHM and a pulse width of 181 fs FWHM. Figure 8 shows the corresponding (manufacturer-measured) optical spectrum and auto-correlation trace of the fiber laser.

Another issue related to the use of low-repetition-rate OMO is the early saturation of the photodiode. Since the saturation behavior of photodiodes is limited by the pulse energy, they tend to saturate with lower average power at lower repetition rate, which limits the available signal-to-noise ratio of the photo-generated RF signal. As a recommendation for future improvements, an OMO operating at higher harmonics of 68 MHz may be beneficial.

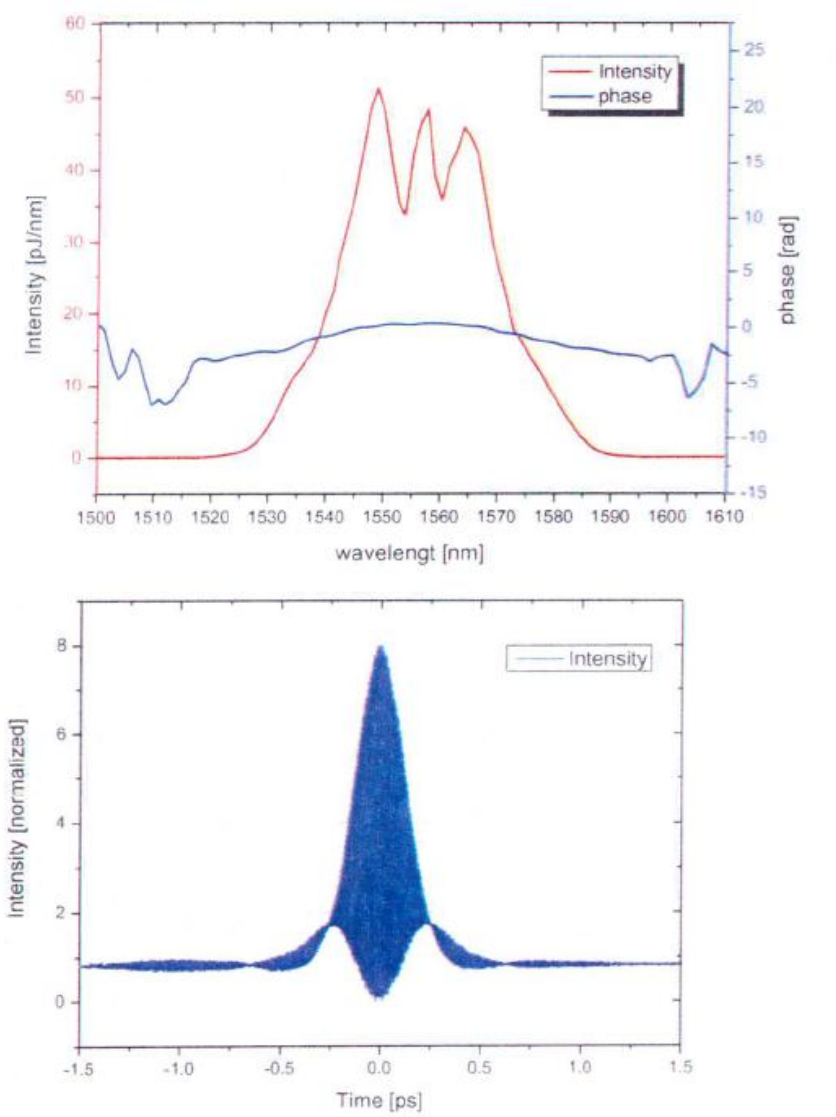

Figure 8 - Optical spectrum (above) and autocorrelation trace of the modified FemtoErb 1560 fiber laser after custom modifications to operate with a narrower the optical spectrum, i.e. longer pulses.

III.2. Development of Two-Color Balanced Optical Cross-Correlator (TCBOC)

In order to optically synchronize the Ti:sapphire lasers in the laser room and the experimental hutch to the OMO, the BOC from phase I of the STTR needed to be adapted to produce an error signal from two different lasers centered at 1550 nm and 800 nm. The challenges here are not only in the two-color design but also in making the device long term stable as the two pulses need to stay overlapped in space and in time. The basic functionality and performance of the TCBOC was verified first with an experimental setup built on an optical breadboard. Based on the test results, IdestaQE has engineered a prototype version that is more compact and mechanically stable. The optical enclosure is milled out of a solid block of Aluminum to ensure

good mechanical stability. The experimental and the final engineered versions of the TCBOC are shown in Figure 9 and Figure 2 above, respectively.

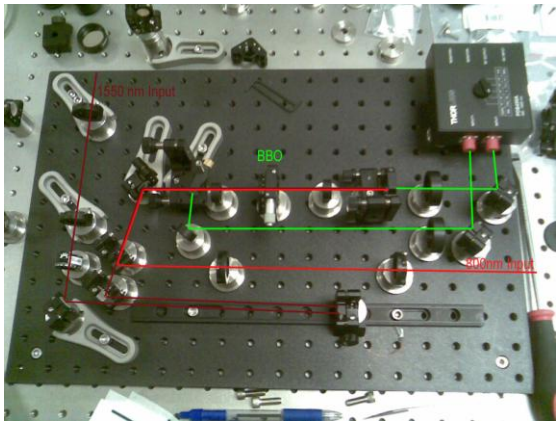

Figure 9 – Experimental (left) and engineered (right) design of two-color balanced optical cross-correlator.

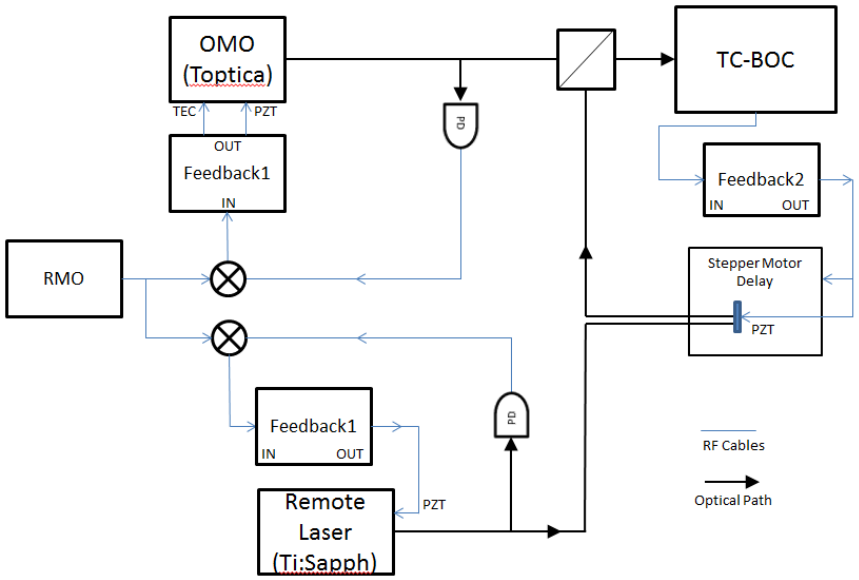

Figure 10 - Feedback and control scheme for synchronization between lasers in the laser room and experimental hutch with IdestaQE's timing distribution system.

Since the TC-BOC only produce error signal when pulses from the two lasers are overlapped in time, the linear region is only present in an extremely narrow window. A two-step locking was adopted in the beginning In order to keep the two lasers in this window. The first step is to synchronize the laser repetition rates with RF feedbacks based on direct photodetection. These first stage feedback loops (feedback loops #1) first suppress the relative timing jitter to about 100fs,and allow pre-locking of the two lasers to a level at which the optical cross correlation can take over and provide synchronization down to the sub 10 fs level (feedback loop #2). Figure 10 shows the block diagram of the control scheme for the TCBOCs. One concern we originally had was that the residual timing jitter from feedback loop #1 was too large, which means that the TCBOC error signal (in feedback loop #2) was not always in its

detection range, which in turn prevented feedback loop #2 from capturing its lock. However, we have later found that the TC-BOC has an auto-locking mechanism by creating a potential well that snaps the pulse from the slave laser onto the master laser pulses. The pictures below show a step-by-step explanation of how this mechanism works.

STEP 1: Two Laser Pulses Slowly Approach

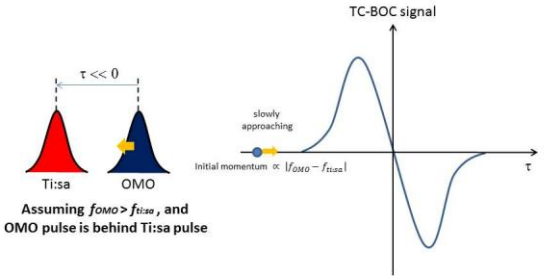

Assuming $f_{OMO} > f_{Ti:sa}$, and OMO pulse is behind Ti:sa pulse

Note: This shows the situation at the BBO crystal, not what you see on the scope.
When two pulses overlap in the crystal, there will be an offset of ~5-6ns on the scope.

STEP 2: Two Pulses Start to Overlap (correct polarity)

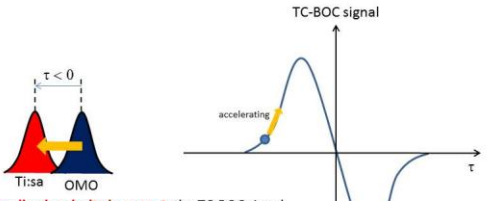

If the **feedback polarity is correct**, the TC-BOC signal will slow down the Ti:sa repetition rate so OMO pulses move toward Ti:sa pulses faster (accelerating). This will give OMO pulse more momentum to climb over the peak of S-curve.

STEP 2: Two Pulses Start to Overlap (wrong polarity)

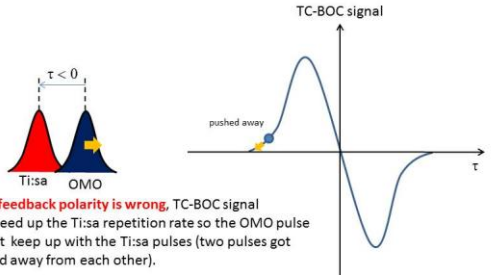

If the **feedback polarity is wrong**, TC-BOC signal will speed up the Ti:sa repetition rate so the OMO pulse cannot keep up with the Ti:sa pulses (two pulses got pushed away from each other).

STEP 3: Deceleration Point

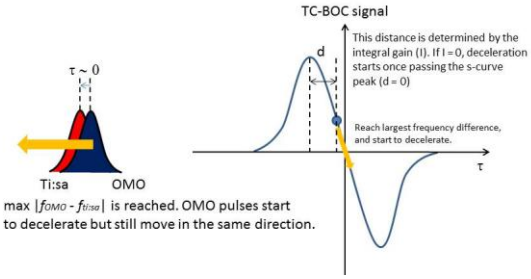

max $|f_{OMO} - f_{Ti:sa}|$ is reached. OMO pulses start to decelerate but still move in the same direction.

Note: If Integral gain (I) is too large, it is possible that the deceleration point happens after passing the zero-crossing point. (To capture the lock easily, use small I gain or turn it off)

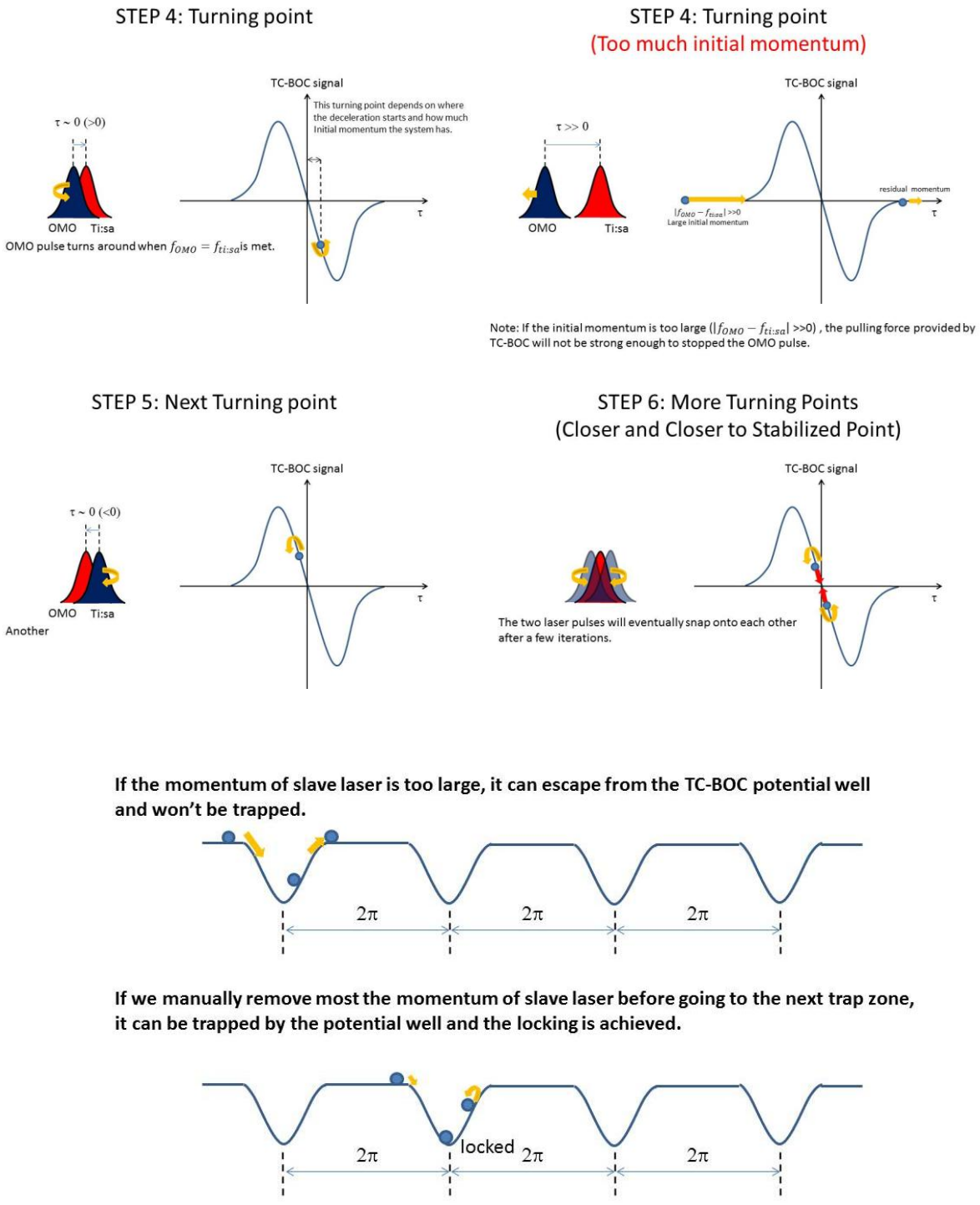

Figure 11 – Step-by-step explanation of the TC-BOC auto-locking theory.

In spite of convenience of the auto-locking mechanism, a pre-synchronization of some manner is still needed for characterizing the s-curve. A useful approach was found by

connecting a function generator to the input of the PI loop. It is then possible to subtract a ramp signal from the TCBOC error signal – in effect sweeping the lock point, or sweeping the 800 nm Ti:Sapphire pulses and the 1550 nm infrared pulses across each other. The cross-correlation in both directions shows a FWHM of ~150 fs. An example of the resulting s-curve (shown in Fig. 12) showed a timing jitter sensitivity as high as 157.2 mV/fs and the linear zone is approximately 120 fs wide.

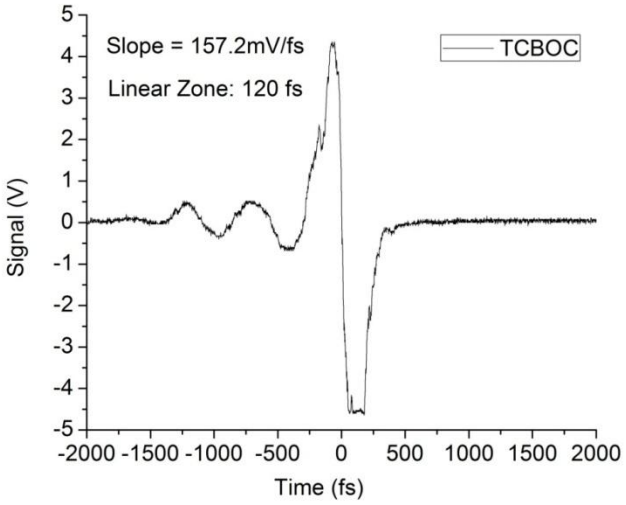

Figure 12 - S-curve of the TCBOC signal

III.3. Balanced Optical-Microwave Phase Detector (BOM-PD)

Tight locking between the RMO and OMO was achieved by a BOM-PD. The BOM-PD is based on electro-optic sampling of the zero-crossings of the rf-signal in a differentially biased Sagnac loop by the pulse train of the OMO. If there is a deviation between the pulse train and the zero-crossings, the BOM-PD gives a low-frequency output proportional to this phase difference. Due to the fact that the Sagnac loop is self-balanced and the electro-optic material making up the modulator has very low thermal drift when compared to photodiodes and microwave mixers, this phase detector has greatly reduced drifts leading to an excellent long term performance. idestaQE has done a custom design for both the optical and RF subsystems for SLAC and implemented the prototype into a 19” rack mount enclosure, along with a dedicated temperature controller which is also rack mountable. The onsite testing of the BOM-PD was done in RLL, the BOM-PD was used to synchronize the Toptica fiber laser OMO to a local Wenzel RMO located inside the RLL. With the control loop disabled, the error signal sensitivity was observed to be ~7 µV/fs, and the corresponding error signal is shown in Figure 13. – The resulting residual phase noise and integrated timing jitter of the OMO when locked to the RMO using the BOM-PD are shown in Fig. 14. The OMO was tightly locked to RMO within 1 kHz

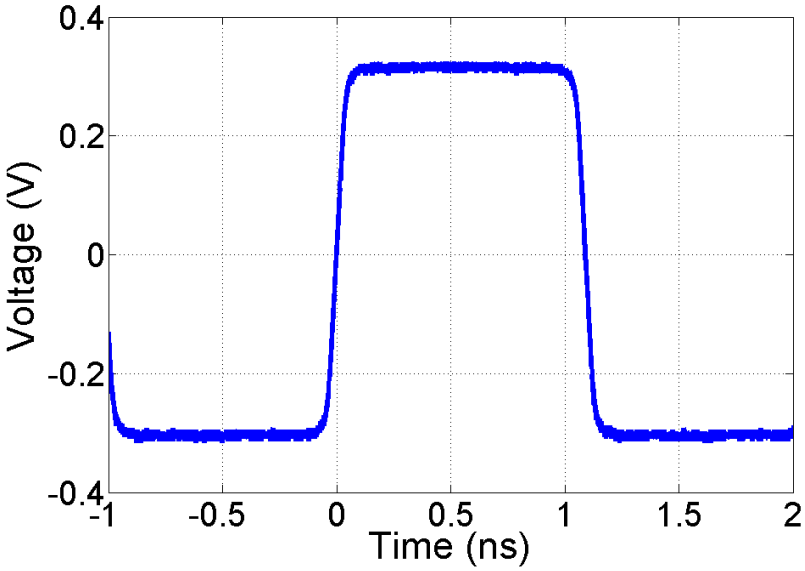

Figure 13 - BOM-PD error signals generated from a local RMO inside the RLL and the Toptica fiber laser OMO.

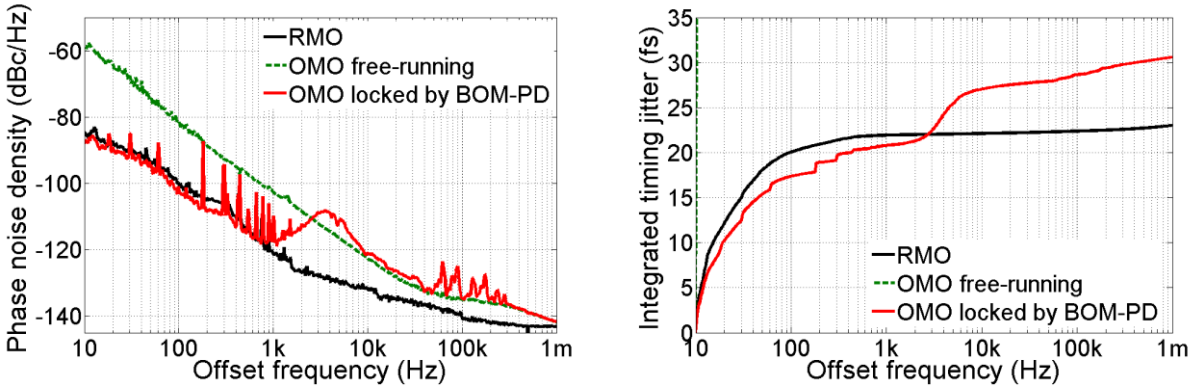

Figure 14 - Residual phase noise and integrated timing jitter of the OMO when locked to the RMO using the BOM-PD.

III.4. Timing Stabilized Fiber Link System (FLS)

The schematic of the newly-designed timing stabilized fiber link is shown in Figure 15. The link is consisting of dispersion-compensated fiber of a few hundred meters long, a PM fiber stretcher and a motorized delay line for fast and slow active control of path length, and an Erbium-doped fiber amplifier for power management. The pulse propagating along the link was partially reflected to the source end and interacts with the newly-emitted pulse from the OMO inside a PPKTP-BOC. The PPKTP-BOC uses a balanced detection approach which is insensitive to amplitude noise of the pulse energy. This design uses piezo-based PM fiber stretcher which can minimize the polarization mode dispersion (PMD) problem. During year 1, we have reviewed the requirement of FLS for SLAC and delivered two PM fiber stretchers, two motorized delay

line devices, a 500-meter dispersion-compensated fiber test link, two compact, portable free-space FLS units and a bidirectional EDFA unit to LCLS for testing.

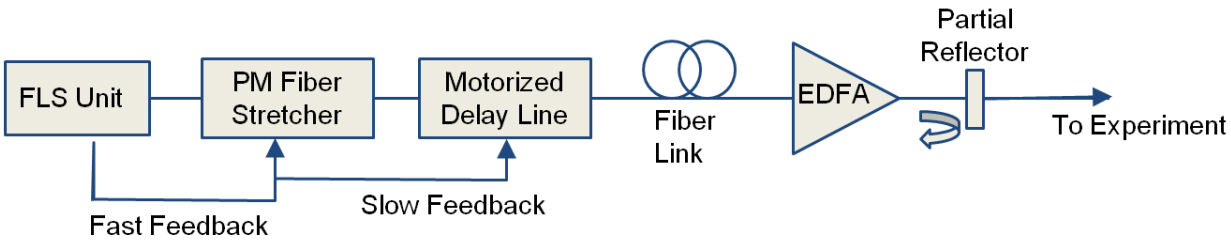

Figure 15 - Schematic of the timing stabilized fiber link.

The single crystal BOC is embedded in the FLS unit, which is the only free-space component in the entire link. As a result, extra mechanical design efforts are required in order to reduce the maintenance needed after the installation. Figure 16 shows the prototype of such device based on a monoblock tray, which minimizes vibration in the free-space components. shows the fiber link receiver box, housing the EDFA and fiber-based partial reflector.

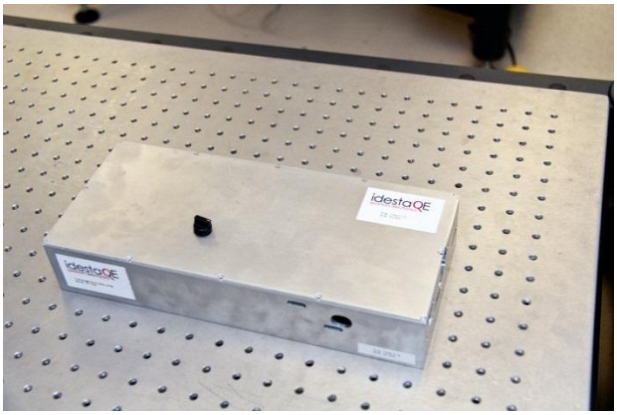

Figure 16 - Prototype of free-space fiber-link-system unit consisting of a balanced optical cross-correlator as a timing detector.

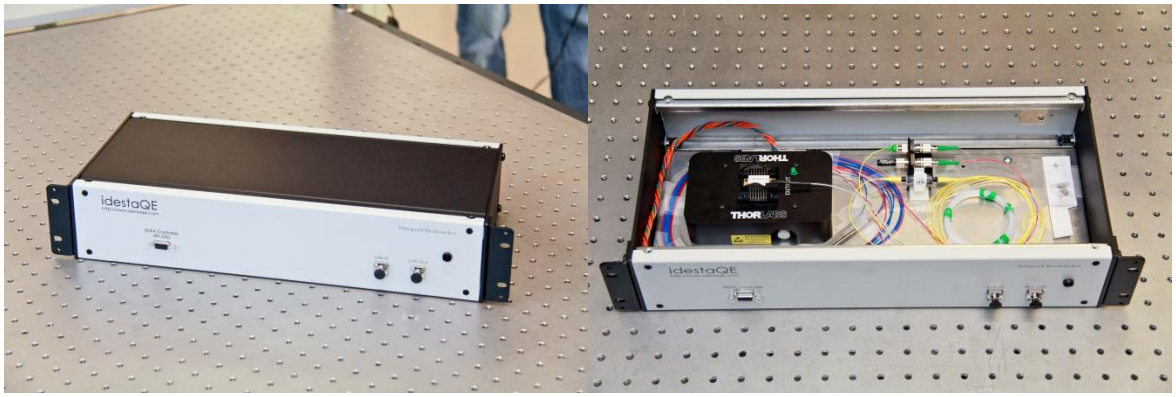

Figure 17 - Fiber link receiver box holding an EDFA for power management and fiber-based partial reflector.

Using the scan function in the motorized delay line, the BOC error signal was generated as shown in Figure 18. The slope sensitivity in the linear region was 4.8 mV/fs and the linear zone is greater than 500 fs. The resulting error signal, with the control loop enabled, is shown in Figure 19. The lock was disabled at ~440 seconds into the experiment, and the timing of the light pulses going through the fiber link is seen to fluctuate significantly. The in-loop residual timing jitter when the lock is enabled is 0.33 fs RMS. However, an out-of-loop PPKTP-BOC was used to verify the residual timing jitter measurement.

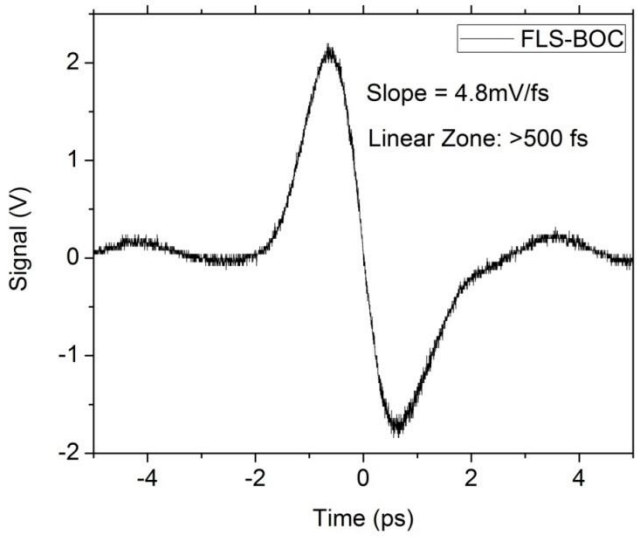

Figure 18 - FLS BOC error signal generated from the back-reflected pulse and the newly generated pulse from the OMO, plotted as a function of time delay.

To verify the basic functionality of the error monitor software, the FLS control loop was tested in a run over a period of over 3.5 hours in order to later measure the long-term timing drift in the fiber link. Fig. 20 shows the MDL position as well as the control loop output voltage logged by the software. It can be seen that the drift over 3.5 hours was ~20 ps. Using a relatively conservative trigger threshold of +/-3V for moving the MDL, the MDL changed positions 471 times during a period of 223 minutes, and the median period between movements is 21 seconds. The manufacturer of the MDL specified a MTBF of 10000 hours in terms of accumulative motor movement, which corresponds to 1.41 years of non-stop travelling.

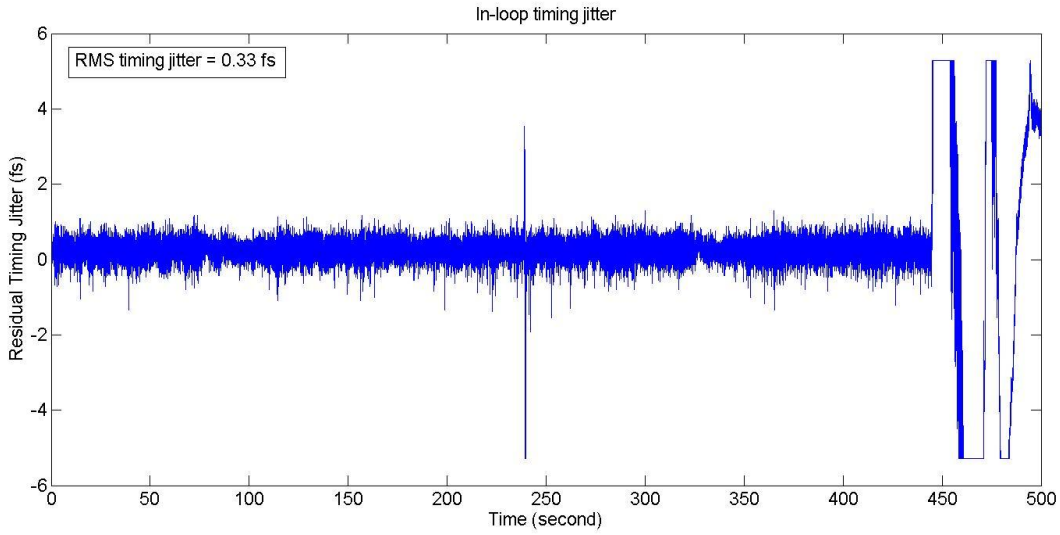

Figure 19 - Error signal of the in-loop PPKTP-BOC when the control loop is enabled. The residual timing jitter is approximately 0.33 fs RMS. The lock was disabled at ~440 seconds into the experiment, and the timing can be seen to fluctuate significantly.

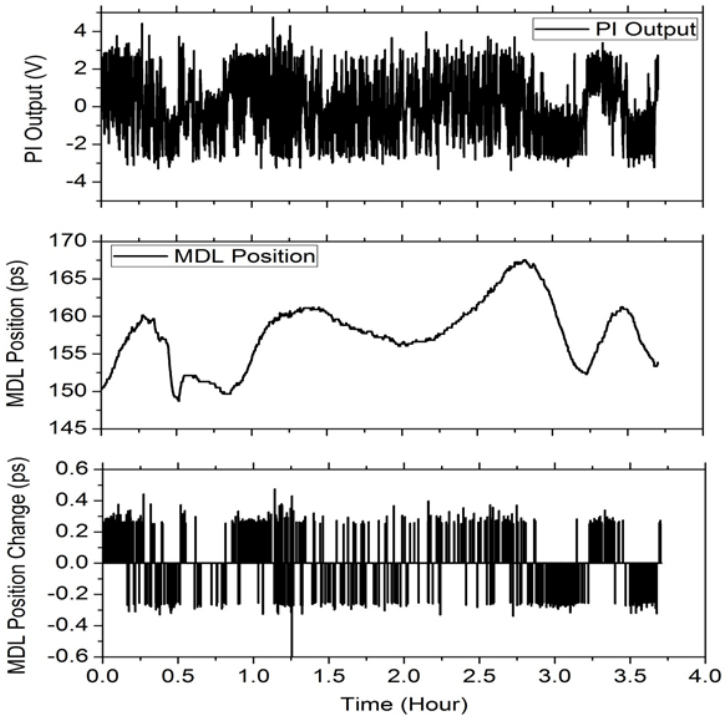

Figure 20 - Test of FLS control loop over 3.5 hours. Control loop output is plotted in the top graph. Motorized delay line (MDL) position is plotted in the middle graph. MDL position changes are plotted on the bottom.

In order to verify the performance of FLS, an out-of-loop experiment was conducted. As shown in Fig. 21, the OMO pulse train was first split into two parts by a 1x2 free-space power splitter. One part was sent to a fiber link made of ~250m of SMF-28 and ~110m of dispersion compensating fiber (DCF-38). By carefully adjusting the input power to the long fiber link, clean S-curves can be produced from both in-loop and out-of-loop PPKTP-BOCs. Both units showed a

sensitivity of ~3.7mV/fs as shown in Fig. 22. The measured residual phase noise from the out-of-loop PPKTP-BOC is shown in Fig. 23. The integrated timing jitter from 1Hz – 10MHz was less than 5fs. The long term stability of FLS was found to be better than 7.6 fs rms over more than 10 days over 360 m long timing stabilized fiber links as demonstrated in the out-of-loop measurements (Fig. 24). We believe a significant portion of these residual timing drifts was from the variations of the uncompensated path length due to environmental changes. Stronger correlation was found between the residual timing errors and the humidity fluctuation of the room. Therefore, better control of humidity of the facility could greatly improve the system performance in the future.

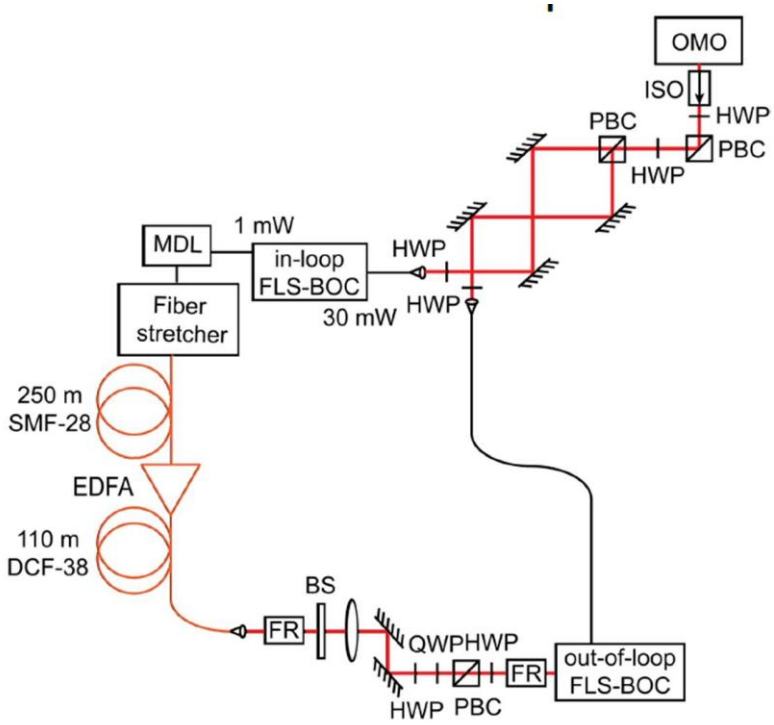

Figure 21 – The experimental setup used for characterizing the out-of-loop performance of the fiber link.

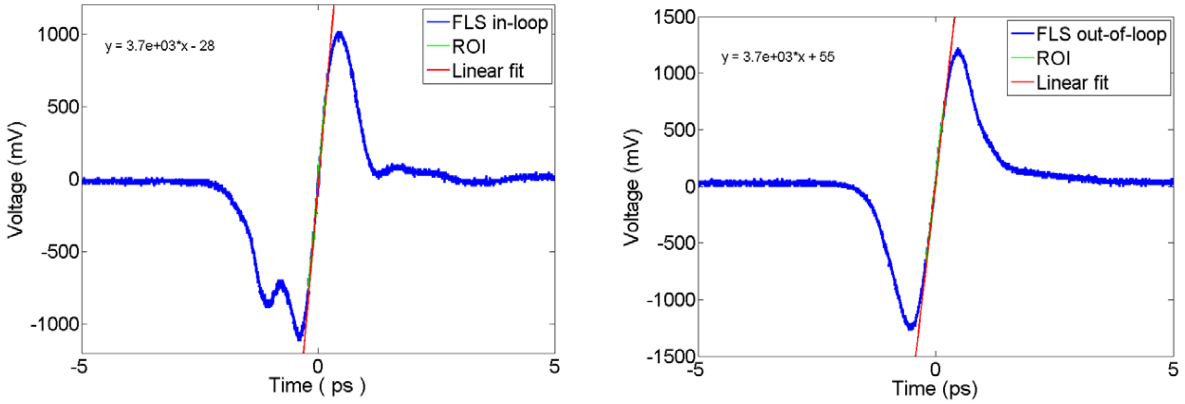

Figure 22 – The S-curve obtained from both in-loop (left) and out-of-loop (right) PPKTP-BOCs. The timing sensitivity of both units was measured to be around 3.7mV/fs.

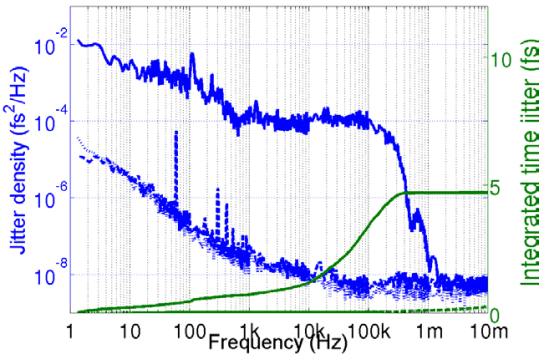

Figure 23 –Out-of-loop residual phase noise and integrated timing jitter of FLS.

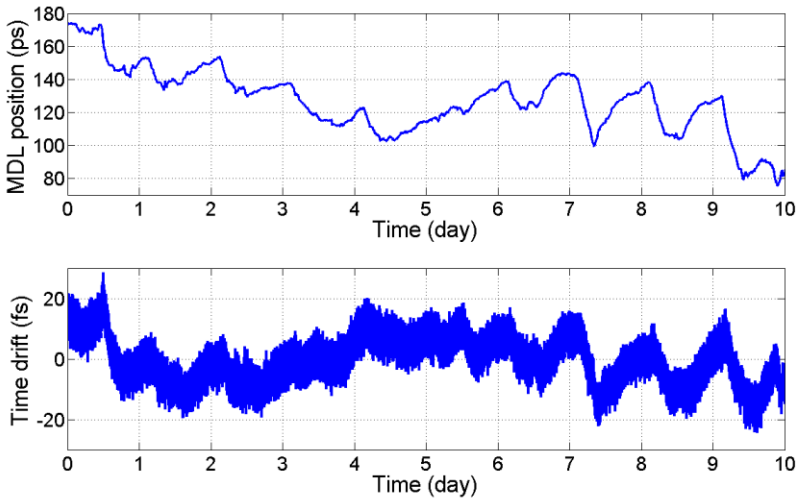

Figure 24 – Measured long-term drifts of a 360m-long timing distribution link. The rms timing drift over 10 days of operation is 7.6fs.

During the second year of the project, the focus was to test two synchronization schemes: (1) Remote optical-rf synchronization and (2) remote optical-optical synchronization. The term "remote" suggests that the slave oscillator is linked to the master oscillator via a timing distribution fiber link of a few 100s of meters.

III.5. Remote Optical-RF Synchronization

Figure 25 shows the experimental setup used to test the remote optical-rf synchronization. Fig. 26 shows the phase noise density for the remote RMO and the synchronized OMO measured with a signal source analyzer. It should be noted that the sensitivity of the BOM-PD was decreased to about 3 μV/fs since the output power of the fiber link became lower in this experiment, which could limit the performance of the synchronization. We were not able to conduct any long-term out-of-loop measurement since only one BOM-PD was built in this project. However, it can be seen that the locked OMO follows the phase noise of RMO at low frequencies and preserves its noise at high frequencies.

In order to further verify the long-term stability of the system, another BOM-PD should be used in the out-of-loop measurement.

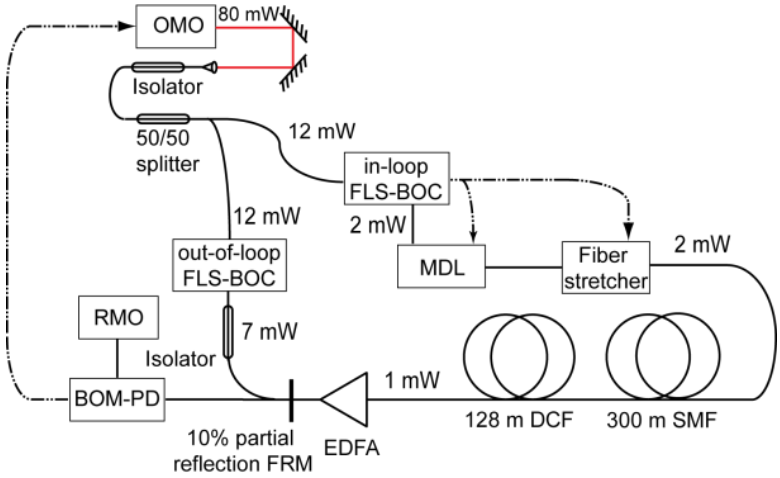

Figure 25 – The experimental setup for remote optical-to-microwave synchronization.

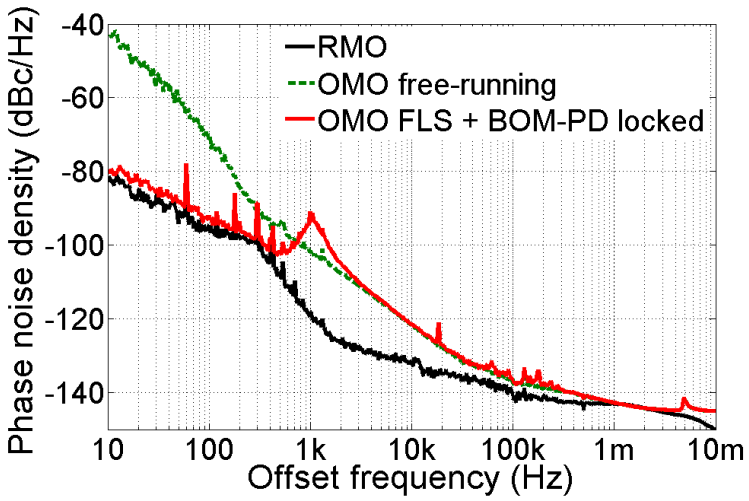

Figure 26 – Phase noise densities (measured with a Agilent signal source analyzer (SSA) at 2856 MHz) of the OMO locked to the remote RMO by the stabilized fiber link system and BOM-PD. The green trace is the phase noise of the free-running OMO; the red trace is the phase noise of the locked OMO; the black trace is the phase noise of the reference RMO.

III.1. Remote two-color optical-optical synchronization

The last but also the most important experiment in this project is the demonstration of remote two-color optical-optical synchronization. In this scheme (see Fig. 27), the OMO was synchronized to the RMO using a BOM-PD, the OMO pulse train was delivered to a remote location through a timing-stabilized fiber link system and used to synchronize a Ti:sapphire laser using a TC-BOC. Another TC-BOC was used for measuring out-of-loop timing error by comparing the pulse train

split from the two oscillators. The sensitivity of the out-of-loop TC-BOC was ~2.6mV/fs and the integrated timing jitter was measured to be less than 13 fs from 1Hz – 10MHz (see Fig. 28). A 3.3fs rms timing drift over 24 hours of operation has been achieved in synchronization of a remote Ti:sapphire laser to the timing of the optical master oscillator (OMO) delivered by a 360 meter long timing stabilized, dispersion compensated fiber link (as shown in Figure 29). To our knowledge, such performance was achieved for the first time in remote optical-optical synchronize scheme.

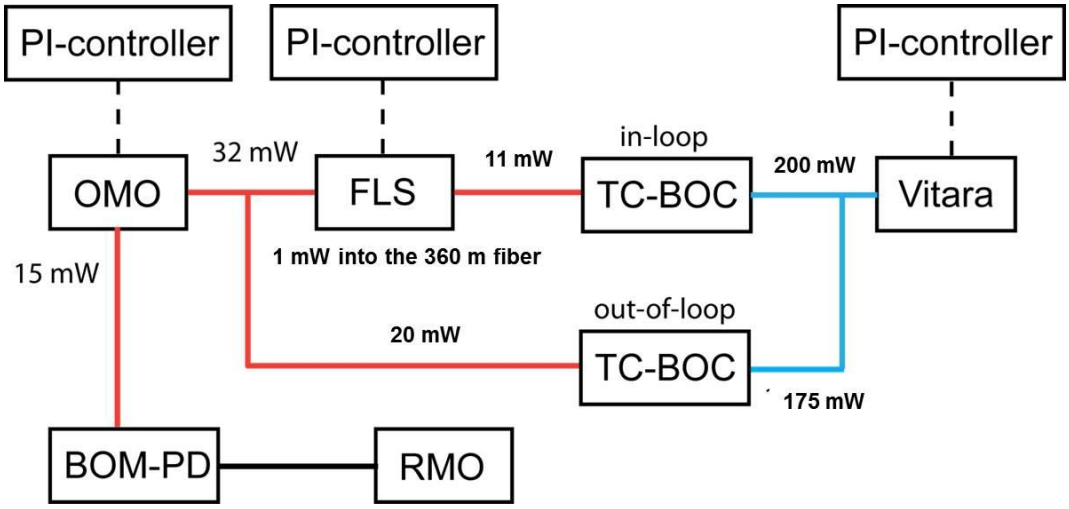

Figure 27 – The experimental setup used for remote optical-to-optical synchronization.

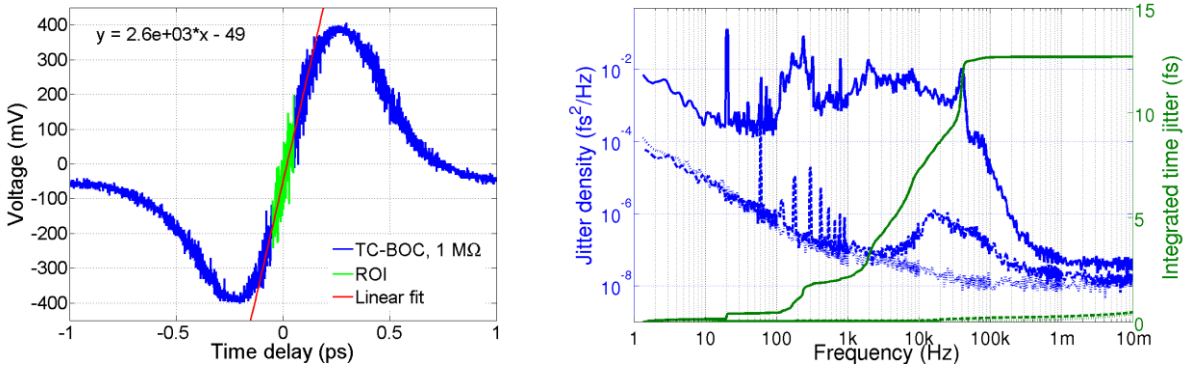

Figure 28 – The S-curve obtained from out-of-loop TC-BOC (left) The timing sensitivity of both units was measured to be around 2.6mV/fs. Residual phase noise and integrated timing jitter obtained from out-of-loop (right) measurements.

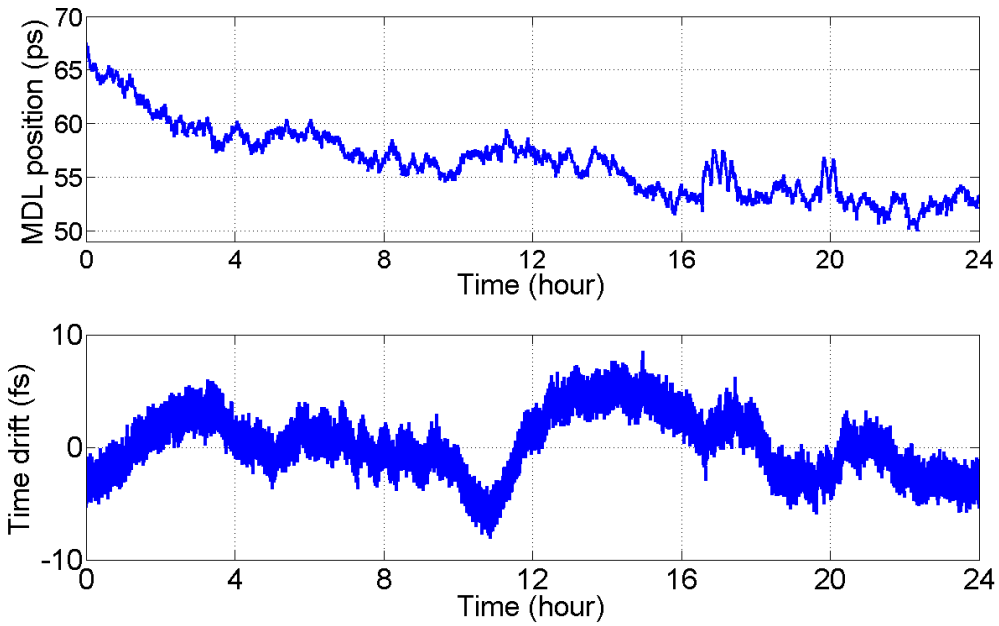

Figure 29 – A 3.3fs rms timing drift over 24 hours of operation has been achieved in synchronization of a remote Ti:sapphire laser to the timing of the optical master oscillator (OMO) delivered by a 360 meter long timing stabilized, dispersion compensated fiber link where the OMO is synchronized to the rf master oscillator (RMO).

IV.Conclusions

In conclusion, we have designed and acquired all key components needed for building a large-scale, sub-10fs timing system for the next-generation light sources. The component-level as well as system-level performance have been verified during this project. For timing distribution, the long term stability of FLS has found to be better than 7.6 fs rms over more than 10 days over 360 m long timing stabilized fiber links confirmed by the out-of-loop measurements. Also for the first time, a 3.3fs rms timing drift over 24 hours of operation has been achieved by synchronizing a remote Ti:sapphire laser to the timing of the OMO through a 360 meter long timing stabilized, dispersion compensated fiber link. We believe the achievements made in this project will opened up new opportunities for the next-generation light sources as well as the whole laser community.